In situ mineralization of nano-hydroxyapatite on bifunctional cellulose nanofiber/polyvinyl alcohol/sodium alginate hydrogel using 3D printing

Ragab E Abouzeid, Ramzi Khiari, Ahmed Salama, Mohamed Diab, Alain Dufresne, Davide Beneventi

In situ mineralization of nano-hydroxyapatite on bifunctional cellulose nanofiber/polyvinyl alcohol /sodium alginate hydrogel using 3D printing Technology

Ragab E. Abouzeid[1,2,*] Ramzi Khiari[2,3,4], Ahmed Salama[1], Mohamed Diab[1], Davide Beneventi[2], Alain Dufresne[2,*]

[1]Cellulose and Paper Department, National Research Centre, Dokki, Giza, Egypt

[2]Univ. Grenoble Alpes, CNRS, Grenoble INP, LGP2, F-38000 Grenoble, France

[3]University of Monastir, Faculty of Sciences, UR13 ES 63 - Research Unity of Applied Chemistry & Environment, 5000 Monastir, Tunisia.

[4]Higher Institute of Technological Studies of Ksar Hellal, Department of Textile, Tunisia

*Corresponding author. Email: r_abouzeid2002@yahoo.com; alain.dufresne@grenoble-inp.fr

Graphical abstract

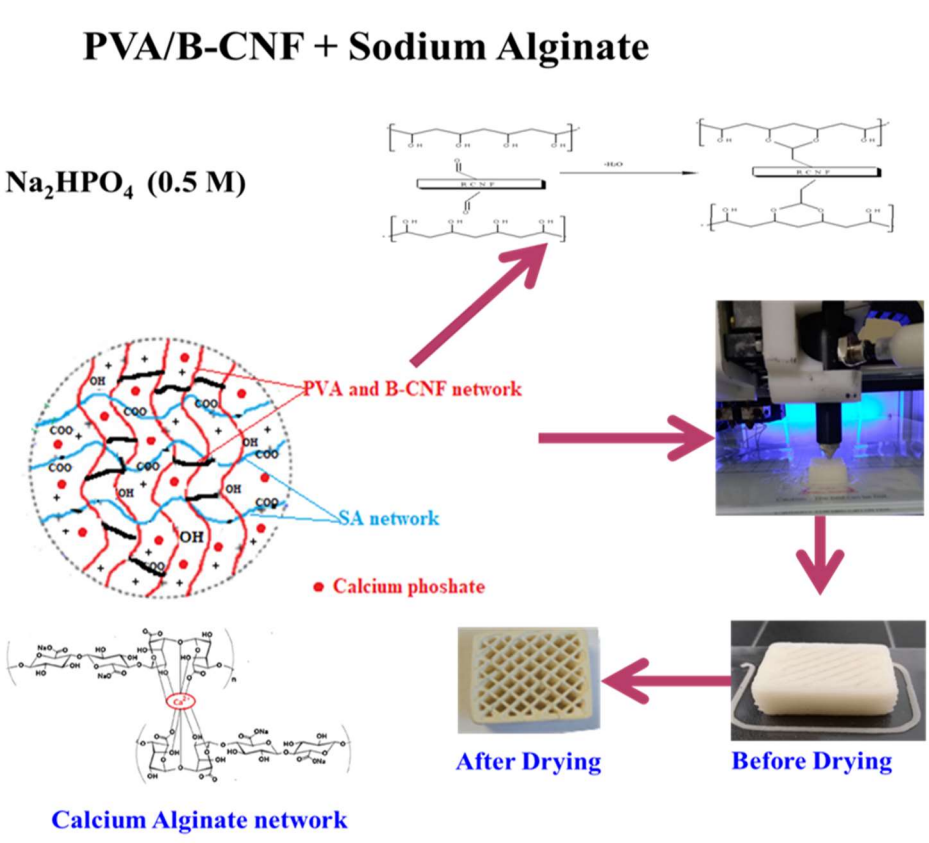

Abstract

This paper describes the manufacturing of scaffolds for the in-situ mineralization of hydroxyapatite using aqueous suspensions of alginate and polyvinyl alcohol-grafted cellulose nanofiber and and 3D printing. Bifunctional cellulose nanofibers (CNF) with carboxyl and aldehyde moieties were prepared starting from bleached bagasse pulp and crosslinked with Polyvinyl alcohol (PVA).Aqueous hydrogels for 3D printing were prepared by direct mixing PVA-grafted CNF with sodium alginate with and without the addition of phosphate ions. A calcium chloride solution (with 0.1 $mol.L^{-1}$ of Ca^{2+}) was sprayed during the printing process in order to partially crosslink alginate and to increase the dimensional stability of the printed gel. At the end of the printing process, the prepared scaffolds were dipped into a $CaCl_2$ solution (0.5 $mol.L^{-1}$ of Ca^{2+}) to: i) complete alginate cross-linking and ii) promote hydroxyapatite nucleation and growth by reaction with phosphate ions. In order to better understand mechanisms governing scaffolds manufacturing by 3D printing, the rheological behavior of alginate/PVA-grafted CNF and the mechanical properties of unit filaments obtained by direct hydrogel extrusion Final scaffolds were characterized by several techniques namely: SEM, FTIR and TGA. This study demonstrates that sodium alginate/PVA-grafted CNF hydrogels are promising materials for manufacturing scaffolds for bone tissue engineering by 3D printing.

Keywords: Cellulose nanofibril; Alginate hydrogel; Nano-hydroxyapatite; 3D printing technology.

Introduction

In recent years, 3D printing became an encouraging technology for the production of nanocomposites for bone tissue engineering. In-situ biomimetic mineralization of hydroxyapatite/3D scaffold is one of the most important applications of biomaterials to replacemedamaged hard tissues and repairbone defects [1]. Several biomaterials can be used for preparation of bone tissue scaffolds. These biomaterials should have some of requirements such as biocompatibility, biodegradability, suitable mechanical strength and low cytotoxicity [2,3]. Synthetic polymers, such as aliphatic polyesters, have been extensively investigates and tested, i.e.: Polylactic acid (PLA), poly glycolic acid (PGA), poly-ε-caprolactone (PCL), polydioxanone (PDO), and polytrimethylene carbonate (PTMC) [4–6]. Nevertheless, natural biopolymers are becoming a valid alternative for thesubstitution of synthetic polymers and collagen, alginate, gelatin and chitosan which are interesting compounds for tissue engineering [2,7] are emerging as outstanding materials for the manufacturing of 3D scaffolds. Alginate is a natural biopolymer, which consists of two monosaccharide units: glucuronic acid and mannuronic acid. Alginate has been also commonly used as scaffold in tissue engineering, drug delivery and cell encapsulation due its biocompatibility, biodegradability and easy gelation with divalent cations under normal physiological conditions [8]. Similarly, cellulose nanofibers (CNF) have gained increased interest in scientific and industrial research because of their unique properties including sustainability, biodegradability, biocompatibility, high surface area, good strength properties, and abundant availability [9–11]. In addition to their physical properties, CNFs can be easily derived from various cellulose sources (such as wood or plant fibers) by using several techniques, i.e. pure mechanical shearing of cellulose fibers or a combination of chemical, enzymatic pretreatments and mechanical disintegration[12]. Owing to their high machanicla properties ans extremely low percolation treshold, CNFs have been effectively used as reinforcing agents for various synthetic and natural polymers [13–15]. Poly

(vinyl alcohol) (PVA) is a biodegradable synthetic polymer, environmentally friendly with good thermal stability, optical properties and high oxygen barrier properties and it is widely used in various applications such as water purification [16] packaging [17] and tissue engineering [18]. In this study, PVA was crosslinked with bifunctional cellulose nanofibers (BF-CNF) with carboxyl and aldehyde groups in order to form stable cyclic acetal bonds with the hydroxyl groups of PVA. PVA-grafted CNFs were blended with alginate to form scaffolds more flexible and softer than those made with pure alginate. In order to evaluate bone precursor nucleation and growth, calcium phosphate was in situ mineralized on 3D porous scaffolds prepared with alginate/PVA-grafted CNFs hydrogels. The effect of pH (4 and 8) on the formation of calcium phosphate was also investigated showing that, in addition to their excellent dimensional stability, the developed scaffolds are homogeneously coated with a mineral layer...

Experimental

Materials and Methods

Cellulose nanofibers were prepared from bleached bagasse pulp which was supplied from Quea Company of Paper Industry (Egypt). All the chemical reagents (Hydrolyzed polyvinyl vinyl alcohol (PVA), sodium alginate (SA), sodium periodate ($NaIO_4$), NaBr and 2,2,6,6-tetramethylpiperidine-1-oxyl (TEMPO)) were purchased from Sigma Aldrich and were used with no further purification.

Preparation of bifunctional cellulose nanofiber (BF-CNF)

TEMPO oxidized of bleached bagasse pulp was prepared according to a previously published method [7,19]. The first step consists in dispersing the bleached bagasse pulp (5 g) in 500 ml of distilled water with 0.08 mg (0.5 mmol) of TEMPO and 0.8 mg of sodium bromide (8 mmol).

Then, 50 ml of sodium hypochlorite solution was added under stirring and the pH was adjusted to 10. At the end of reaction, the pH was adjusted to 7 and the product was centrifuged at 7000 rpm during 30 minutes. The obtained modified fibers were further purified by several centrifugation cycles, i.e. the sediment was collected, diluted with distilled water and centrifuged. Finally, the modified cellulose was purified by dialysis for one week against deionized water. After the TEMPO reaction, the product was defibrillated with a Masuko girder in order to obtaining T-CNF. Periodate oxidation of T-CNF was carried out according to a procedure described previously. 12 g of T-CNF diluted to 1 % consistency was heated to 60 °C in a water bath, 46 mmol of sodium periodate ($NaIO_4$) was added and the reaction container was covered with an aluminum foil to avoid periodate photo-induced decomposition. The reaction was stopped after 3h by washing the resulting dialdehyde cellulose nanofiber with distilled water and filtering it in a funnel. The aldehyde content of oxidized cellulose was then determined [20].

Characterization of BF-CNF

Several technical methods were applied to characterize the BF-CNF namely: FTIR, atomic force microscopy (AFM), optical microscope and UV-visible spectroscopy. The carboxylate content of oxidized cellulose was also determined by conductimetric titration.

Preparation of Alginate Filament using 3D Printing

2.5 g of polyvinyl alcohol were dissolved in 0.5 mol L^{-1} of Na_2HPO_4, then 0, 5, 10 and 15% of bifunctional cellulose nanofiber (with respect to the PVA content) were added. The pH of the solutions was adjusted to 4 using a 0.1 mol.L^{-1} HCl solution and vigorously mixing it for 4 hours at 40°C. 5 g of sodium alginate were added to the previous solutions while keeping the mechanical stirring. The mixed pastes were filled into a 50 mL plastic syringe with a diameter of 15 mm. A metal nozzle with an end diameter of 0.5 mm was connected to the syringe and

the syringe was placed in an in home modified 3D printer (Leapfrog, Creatr HS model) connected with a screw-pump paste extruder (Wasp, claystruder).The extruded PVA/alginate filaments were printed in a cylindric flask filled with a $CaCl_2$ solution in order to cross-link alginate. The extrusion head speed was set to 1000 $mm.min^{-1}$ and the hydrogel syringe was fed with a pressure of 0.5 bars. The width of the filament and the layer height were set 0.6 mm and 0.35 mm, respectively. The extruded filaments were left in the flask for 2 min after that the filaments were putted in straight line.

Mechanical Testing of the filaments

The prepared filaments were air dried and conditioned at 50% relative humidity for 3 days before tensile testing. Tensile testing was performed with an Instron model 5569 with a load cell of 5 kN and a crosshead speed of 10 $mm.min^{-1}$. The diameter of the filament after air drying was measured using a ZEISS Stereo Discovery V20 with an AxioCam ICc 5. The images obtained were analyzed using the image J "Analyze stripes v2.4.5.b" plugin to measure the filament diameter. Blue hill software was used for test control and collection of the data. The data received were used to calculate the modulus of elasticity which taken from the slope of stress-strain curves. Five samples were tested for mean and standard deviation calculation.

Rheological Characterization

The rheological behavior of all the prepared hydrogels were determined using a MCR 301 rheometer (Anton Paar). A parallel plate with 25 mm diameter was used and the gap distance was set to 1 mm. The cover was used to prevent water evaporation during measurements, and the temperature was maintained at 23 °C. The samples were equilibrated 1 min to remove any previous shear history. Viscosity was measured with shear rate ranging from 10^{-3} and 10^{3} s^{-1}. The viscoelasticity of all materials was examined and the linear viscoelastic region (LVR) was concluded by amplitude sweeps conducted at the frequency of 0.5 Hz and strain from 0.1-100%.

Preparation of 3D scaffolds and mineralization

3D scaffold with cuboid shape and nominal size of 20*20*10 mm were printed. It is important to mention that a solution of $CaCl_2$ (0.05 $mol.L^{-1}$) was sprayed after each layer to induce a partial alginate crosslinking and strengthen the hydrogel. Afterwards, all of the fabricated scaffolds were soaked in 0.5 $mol.L^{-1}$ $CaCl_2$ in order to complete alginate crosslinking and to promote the in situ mineralization of calcium phosphate. The pH was adjusted, directly after mixing, to 4 and 10 using 0.1 $mol.L^{-1}$ NaOH and HCL. The mixtures were stirred smoothly during three days at room temperature. Milky white materials were produced immediately on the surface of the fabricated scaffolds due to the formation of calcium phosphate. The crosslinked scaffolds were thoroughly washed by deionized water for three times and freeze dried for further characterization.

Characterization of 3D scaffolds

The surface morphology of the prepared scaffold before and after mineralization was imaged using a scanning electron microscope (FEI-Quanta 2000, ESEMTM) equipped with a EDX Unit (Energy Dispersive X-ray Analyses). 10 mg of material were mixed with 300 mg of KBr in order to prepare discs for Fourier Transformed Infrared Spectroscopy. The range of length wave was from 4000 to 500 cm^{-1} with a resolution of 4 cm^{-1} and an accumulation of 16 scans per analysis. FTIR spectra were recorded using a Perkin Elmer FT-IR spectrometer (Perkin Elmer, USA). The thermal properties of the prepared samples were determined by thermogravimetric analysis. The analysis was done using the PerkinElmer TGA thermogravimetric analyzer under air flux from 25 to 800 °C with a heating rate of 10 min^{-1}.The analyses were conducted in duplicate. X-ray powder diffraction was carried out on of finely grinded scaffolds, before and after mineralization, at the MCX beamline at Elettra-Sincrotrone Trieste, Trieste, Italy [21,22]. The sample was poured in a thin walled borosilicate glass

capillary with a diameter of 1.0 mm. The wavelength used for the data collection was 0.827 Å and the data were collected in the 2θ range (3 – 50°). In order to improve particle distribution statistics, the capillary was rotated during the XRD diffraction

Results and discussion

Scheme 1 presents the different steps of the production bifunctional cellulose nanofibers (BF-CNF) using chemical and mechanical treatments. The first step consists in the TEMPO oxidation of cellulose fibers and the generation of carboxyl groups at C6 position. The second step corresponds to the mechanical defibrillation of oxidized fibers and the production of cellulose nanofibers (T-CNF). In the last step T-CNF are periodate oxidation induces the formation of dialdehyde moieties in position C2 and C3 with the cleavage of the C2-C3 bond. The carboxylate content of T-CNF, which was 0.9 $mmol.g^{-1}$ (as estimated by conductimetric titration),slightly increased after the periodate oxidation, whereas the aldehyde reached 2.5 $mmol.g^{-1}$.

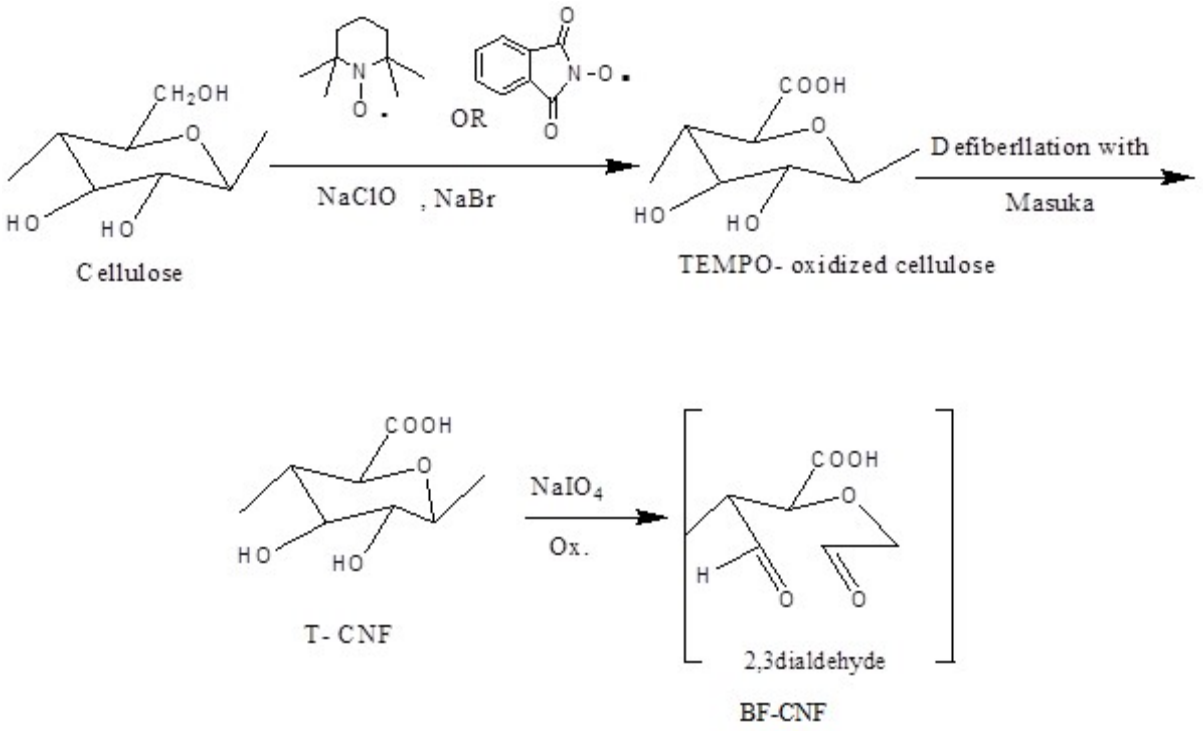

Scheme 1. The synthesis of bifunctional cellulose nanofiber with aldehyde and carboxylic acid groups.

Characterization of bifunctional cellulose nanofiber

FT-IR spectra shown in Fig. 1 confirmed the effective oxidation of cellulose by TEMPO and Periodate . After TEMPO oxidation, a new band, corresponding to the C=O stretching of carbonyl groups, was detected at 1743 cm^{-1} . Significant increase in the carbonyl groups band was observed after periodate oxidation of TEMPO cellulose due to the formation of aldehyde groups.Peaks at around 880 cm^{-1} are assigned to the formation of hemiacetal bonds between the carbonyl groups and neighbor hydroxyl groups corresponding at the C1 position. The BF-CNF was also examined by e AFM andimages are shown the Fig.1.A and B. It can be noticed that nanofibers become thinner and shorter, which can be attributed to a loosen adhesion between microfibrils and the electrostatic repulsions between the surface charges.

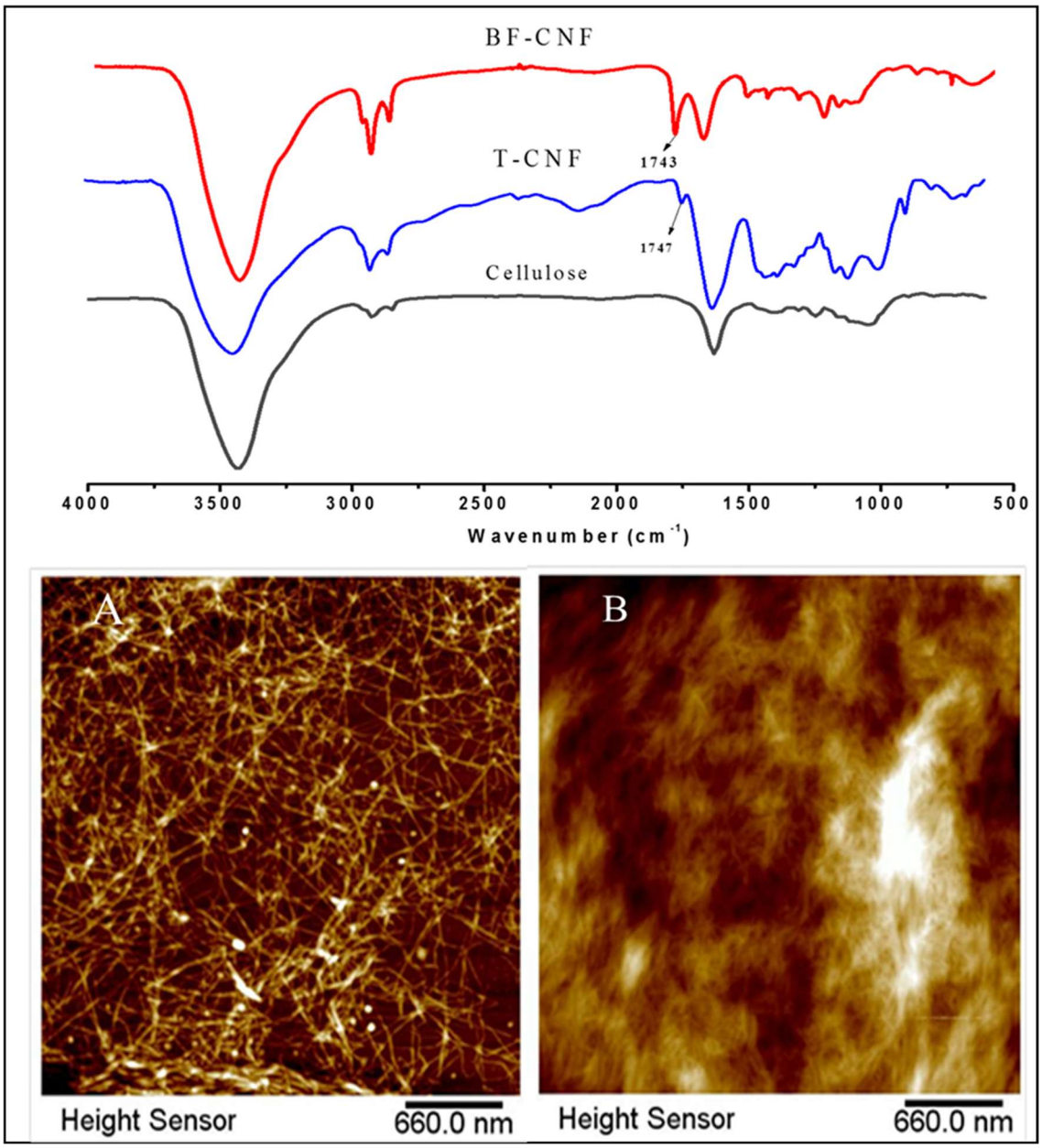

Figure 1. Spectra of FT-IR of cellulose, T-CNF and BF-CNF, AFM images of T-CNF (A) and BF-CNF (B).

This study shows the use of bifunctional cellulose nanofibers (BF-CNF) as a potential crosslinking of polyvinyl alcohol with the formation of stable acetal bonds between the hydroxyl groups of PVA and the aldehyde groups of BF-CNF as represents by figure 2.

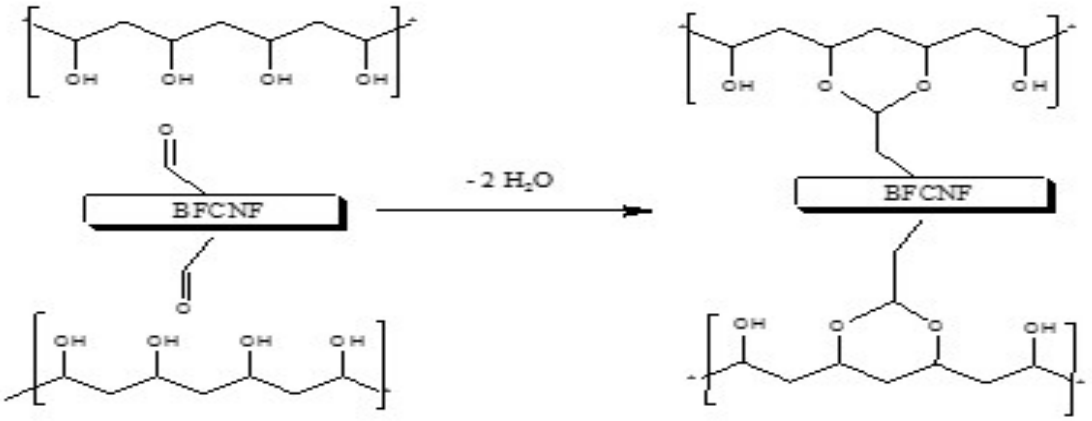

Figure 2. Schematic illustration of the acetal crosslinking of PVA with the aldehyde groups of BF-CNF.

Rheological Characterization

The rheological properties of different PVA/SA hydrogels with different percentage of BF-CNF were investigated at 23°C to investigate how the viscosity changes with the shear rate during printing the process at room temperature. The Viscosity of all hydrogels was measured with shear rates ranging from 0.01−1000 s^{-1}. Figure 3A shows that all prepared hydrogels display a shear-thinning behavior with viscosity decreasing when increasing the shear rate [23,24]. This behavior can be associated to the typical disruption of the hydrogel nanofiber network at high shear rates. The increase of the BF-CNF fraction (with respect to PVA) led to higher viscosities which were correlated with the dense entanglement among nanofibers. The linear viscoelastic region (LVR) and the yield stress of the prepared hydrogels were determined using amplitude sweep. at a constant frequency of 1 Hz. At low strain values, the storage modulus (G') and the loss modulus (G″) were independent from the strain amplitude and the storage modulus had higher values than the loss modulus thus indicating prepared hydrogels are very structured. Athigh strain values the storage modulus progressively decreased revealing hydrogel destructuration and the transition from an elastic to a viscous behavior when G'/G″ < 1. The critical strain (γc), corresponding to the transition from the linear viscoelastic region

to the viscous region (i.e. the point where G' shows 5% reduction from its LVR value) [25][26]was lower than 1 % for most of the prepared hydrogels. Therefore, a strain value of 0.5 % was selected to study the linear viscoelastic behavior of the prepared hydrogels in order to avoid hydrogel destructuration. Among tested hydrogels, the PVA/15%BF-CNF/SA displayed the highest storage modulus, which was in line with a denser cross-linking and a higher nanofiber concentration.

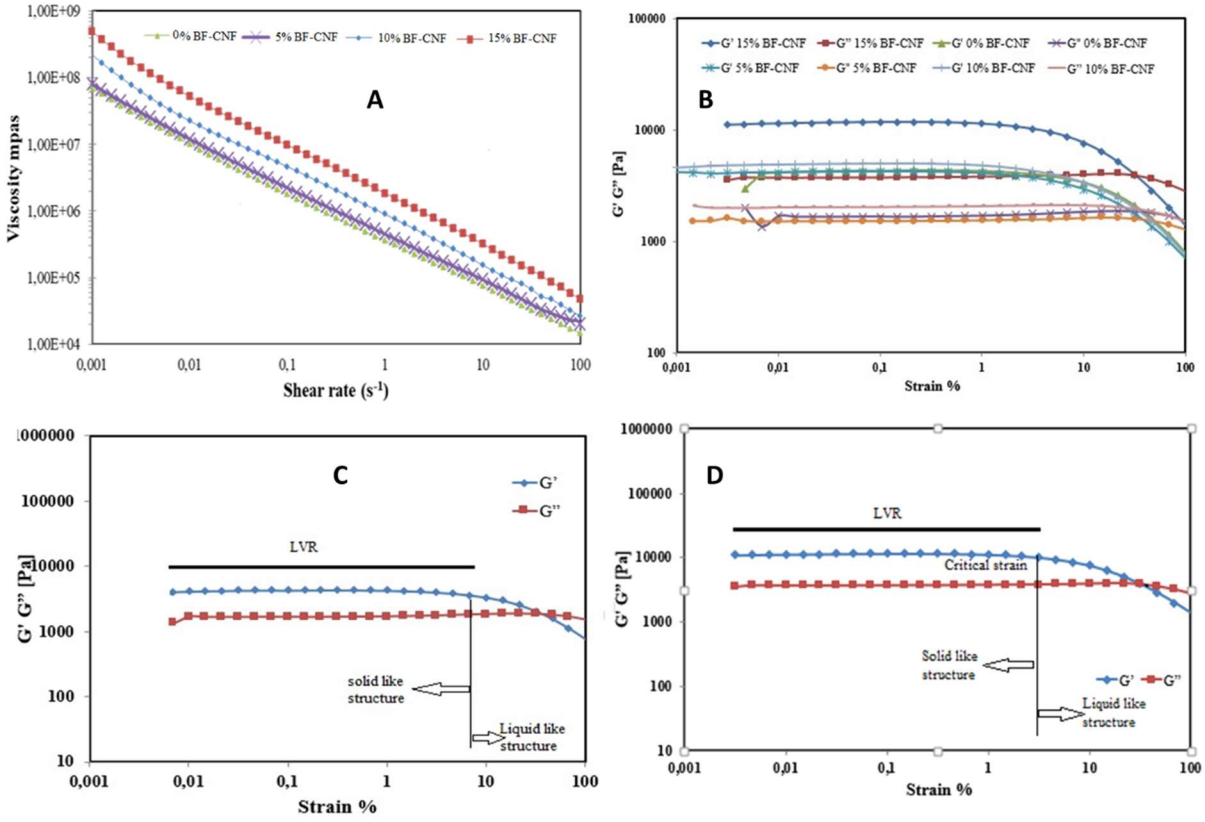

Figure 3. (A) Viscosity vs. shear rate plot of the various hydrogel formulations performed at 23 °C. B) Strain sweep study for the various hydrogels at 1 Hz: evolution of the storage modulus G′ and loss modulus G″.(C and D) strain sweep study for PVA/SA and PVA/15%BF-CNF/SA at 1 Hz; evolution of the storage modulus G′ and loss modulus G″ respectively.

Tensile Properties of PVA/BF-CNF/SA filaments

Figure 4a presents the stress-strain curves of bare filaments as a function of the BF-CNF concentration. The addition of BF-CNF to the pristine hydrogel induced a drop of the strain at break from ca. 4% to 1.5% and an increase of the stress at break and Young modulus from 20 MPa and 0.5 GPa to 20-25 MPa and 2.5 GPa, respectively. The neat increase of the dry filament mechanical properties and the shift to a brittle behavior was interpreted as reflecting the formation of a dense CNF network even in the presence of a low BF-CNF frction.

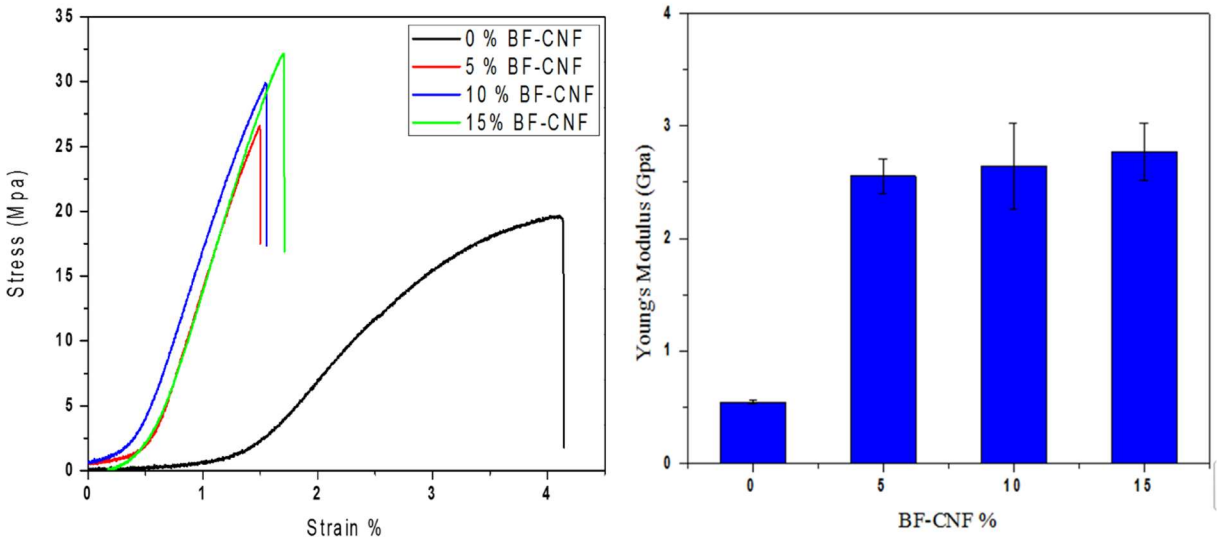

(a) **(b)**

Figure 4. Typical (a) stress-strain curve and (b) Young modulus of air-dried filaments containing different fractions of BF-CNF.

Fabrication and Characterization of 3D Scaffolds.

Figure 5 shows 3D scaffolds (20×20×8 mm) prepared in wet state (A and B) and freeze dried after soaking in (C) water(control sampler) and (D) in $CaCl_2$ solution. Figure 5(C and D) show that sample soaking in the $CaCl_2$ solution induced the generation of a rough surface and a slight increase in the diameter of the bare filament. Whereas, there was no apparent visible change in the control sample with water solution (Figure 5C). These morphological changes were ascribed to the reaction between calcium and phosphate ions on the surface of dry filaments composing the printed scaffold.

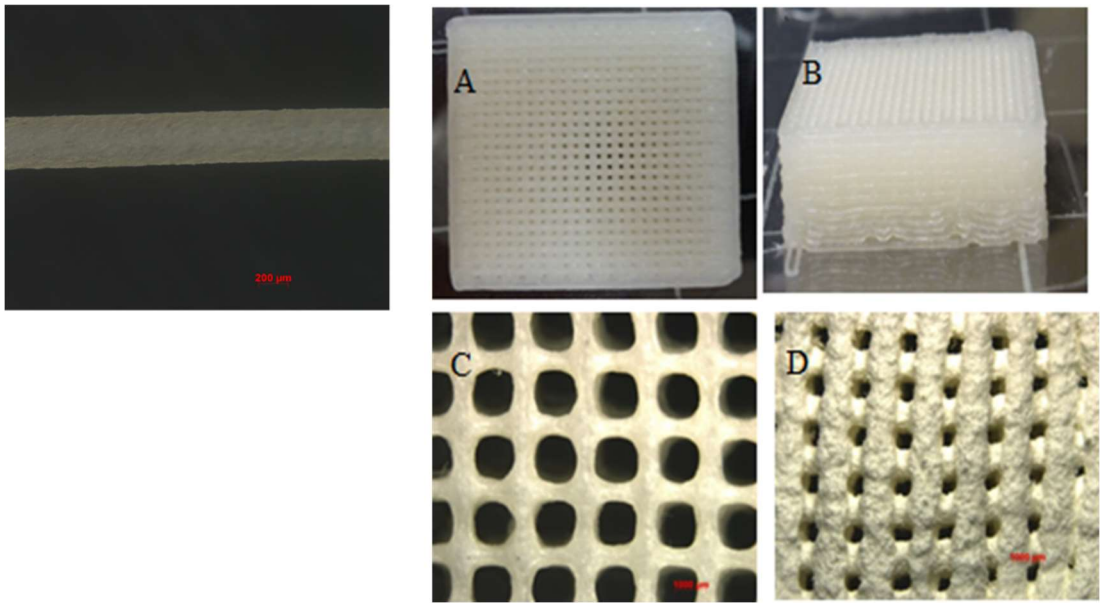

Figure 5. Photographs of 3D printed scaffolds20x20x8 mm prepared with 0.5 M Na_2HPO_4 (A and B). Microscopic images of 3D printed alginate/PVA scaffolds C) without 0.5 M Na_2HPO_4 and D) with Na_2HPO_4 soaking in $CaCl_2$ solution.

Indeed, FTIR spectra of the prepared scaffolds with and without addition of Na_2HPO_4 (B and C) at different pHs (4 and 8) revealed the presence of the absorption bands typical of the P–O stretching vibration mode ν3 at wavenumbers 1160 and 1049 cm^{-1}, O–P–O bending vibration mode ν4 at 550 and 600 cm^{-1} and P–O mode ν1 at 894 cm^{-1} compared to PVA/SA scaffolds (A)

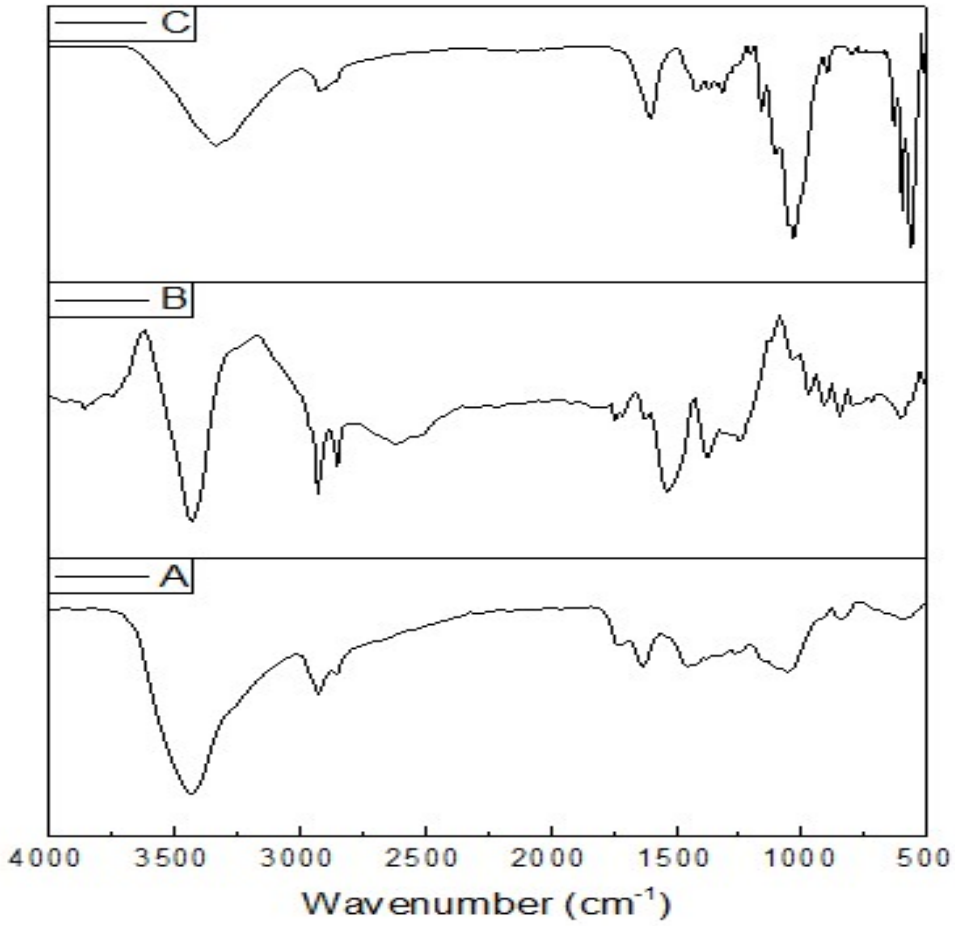

Figure 6. FTIR absorption spectra of prepared scaffolds with water (A) and with 0.5 mol. L^{-1} Na_2HPO_4 at pH 4 (B) and pH 8 (C).

XRD spectra of the formed PVA/BF-CNF/SA/calcium phosphate hybrids at different pHs (Figure 7)displayed a broad peak at 2θ(°)=10.3 which is a common peak of polysaccharides, i.e. cellulose and alginate in the current hybrid. Moreover, the formed hybrid at pH 8 showed the characteristic signals 2θ (°) = 26, 27.8, 32.9, 39.0 and 43.6 which are associated with the diffraction pattern of hydroxyapatite. In contrast, calcium phosphate precipitated at pH 4 showed reflections at 2θ (°) =11.4, 18.1, 22.1, 25.3, 28.0, 30.9, 34.8, 36.97, that lead to dicalcium phosphate dihydrate (DCPDH) crystal phase formation. Peaks appeared at pH 4 are very sharp reflecting a high degree of crystallinity for the calcium phosphate precipitated on the scaffold surface..

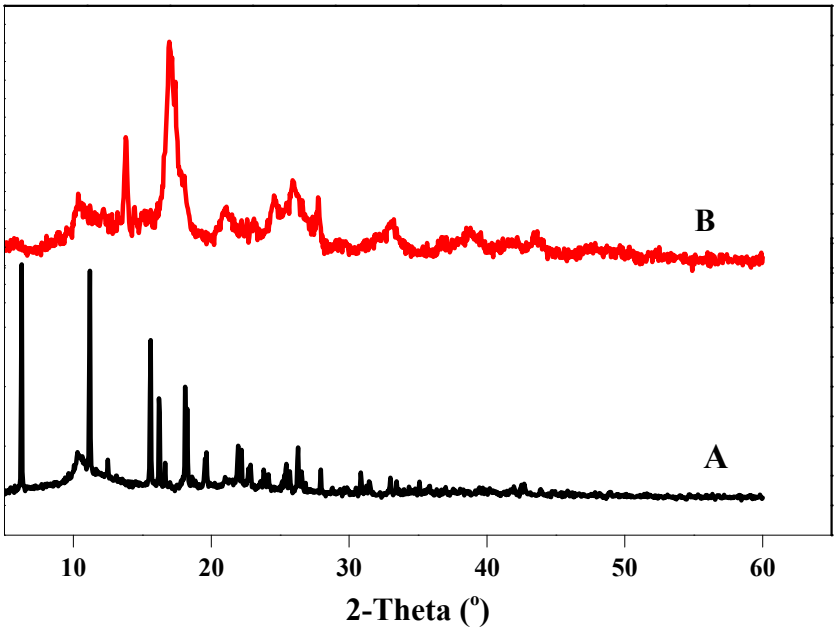

Figure 7. XRD of the formed PVA/BF-CNF/SA/calcium phosphate hybrids at pH 4 (A) and pH 8 (B).

SEM images of the 3D printed and freeze dried PVA/BF-CNF/SA hydrogel shown in Figure 8 confirmed FTIR and XRD spectra. Without calcium phosphate mineralization, Figure 8(A), the sample morphology is relatively homogenous and no clear evidence of a separated phase can be observed. The images of calcium phosphate mineralized in pH 4, Figure 8(B, C) showed large and thin platelets on the surface of PVA/BF-CNF/SA. The size distribution of the crystals is slightly uniform (from ca. 2 to 10 μm) and the crystal shape is well developed. It is also clear that the plates are not existent as individual platy crystals, but they form dense aggregates and display steps and overgrowth of other crystals. In contrast to the hybrid grown in pH 4, the samples developed pH 8 exhibit a relatively uniform porous morphology. This porous structure consists of hierarchical nanoplates (smaller than 100 nm). The effect of pH of the mineralization environment on the morphology of the precipitated calcium phosphate was already reported in the literatures [27,28]. Ahmed Salama et al. [29] observed that the cellulose/calcium phosphate hybrids prepared in the presence of glacial acetic acid where characterized by the presence of

calcium phosphate crystals with a micrometric lamellar structure while in the presence of sodium hydroxide crystals had a uniform structure with nanometric size.

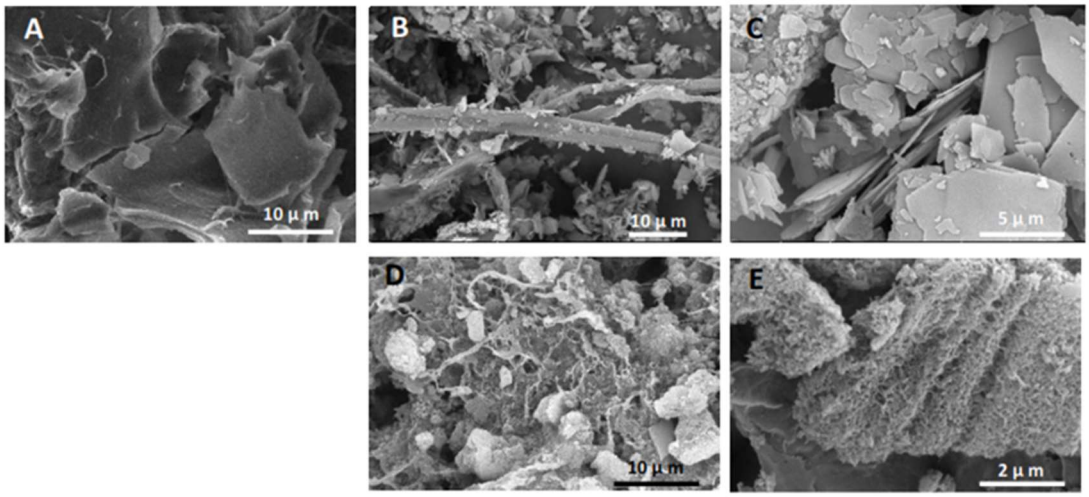

Figure 8. SEM mages of PVA/BF-CNF/SA hydrogel before (A) and after calcium phosphate mineralization at pH 4 (B and C) and pH 8 (D and E).

TGA data of the prepared scaffolds showed that all samples displayed a major weight loss in a temperature range of 220-350 °C which is typical for carbohydrate polymers. At 800°C the weight losse of PVA/BF-CNF/SA in the absence of calcium phosphate (blank) was of 79 % whereas the weight loss of mineralized scaffolds at pH 4 and pH 8 was of ca. 47%. Under the hypothesis of a negligible interaction between the organic and the inorganic phases during the scaffold's pyrolysis, the mass fraction of apatite in mineralized scaffolds at pH 4 and pH 8 can be estimated as 32%, thus indicating the effective crystallization of calcium phosphate

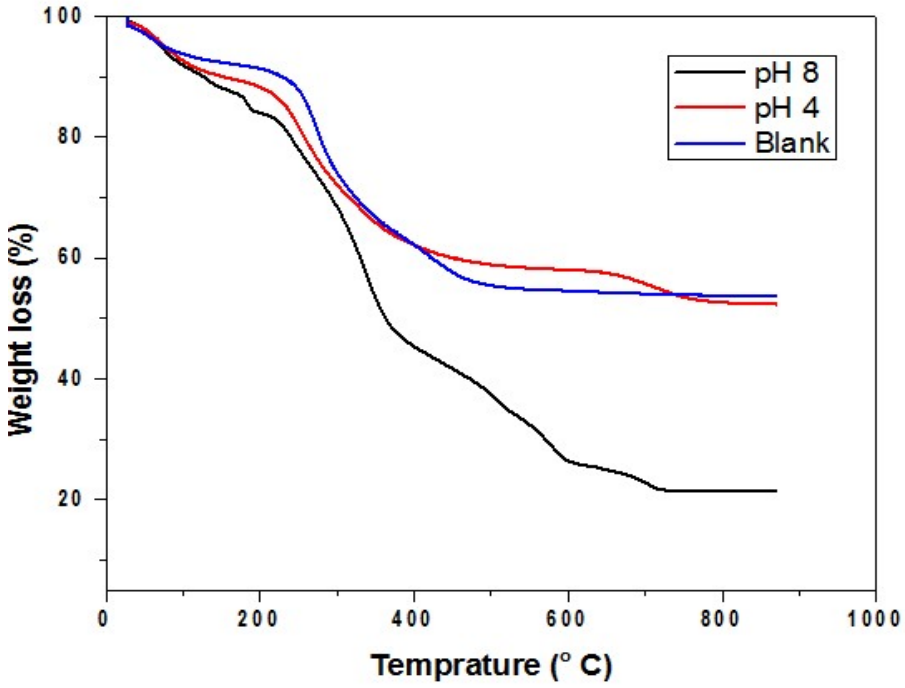

Figure 9. TGA curves of prepared scaffolds: with water (Blank), 0.5 mol $L^{-1}Na_2HPO_4$ at pH 4 and pH 8.

Conclusions

In this work, bifunctional cellulose nanofibers (BF-CNF) were prepared with reactive aldehyde groups and used in the cross-linking the hydroxyl groups of PVA. Cross-linked PVA/alginate scaffolds were fabricated in the presence of Na_2HPO_4 via 3D printing and a subsequent in situ mineralization of calcium phosphate during scaffold cross linking by immersion in a $CaCl_2$ solution. The Young's modulus of cross-linked PVA/alginate scaffolds was increased from 0.54 ± 0.01 GPa with 0%BF-CNF to 2.76 ± 0.26 GPa for 15% BF-CNF. pH had a major effect on the nucleation and growth of calcium phosphate and XRD and SEM analysis showed that the mineral phase in the final hybrid material was was mainly composed by: dispersed lamellar hydroxyapatite at pH 8 and a homogeneous layer of dicalcium phosphate dihydrate (DCPDH) nanocrystals at pH 4. Overall, the prepared PVA/BF-CNF/SA scaffolds with nano DCPDH could be a promising substrate for bone tissue engineering application.

AUTHOR INFORMATION

Corresponding Authors

*E-mail: r_abouzeid2002@yahoo.com

Author Contributions

The manuscript was written through contributions of all authors. All authors have given approval to the final version of the manuscript.

Notes

The authors declare no competing financial interest.

ACKNOWLEDGMENTS

This work was financially supported by the Embassy of France in Egypt − Institut Français d'Egypte (IFE) and Science & Technology Development Fund (STDF) in Egypt (Project No. 30663) as well as to the "PHC-UTIQUE CMCU" (project number 18G1132) for the financial support.

References

[1] Z. Xia, X. Yu, X. Jiang, H.D. Brody, D.W. Rowe, M. Wei, Fabrication and characterization of biomimetic collagen-apatite scaffolds with tunable structures for bone tissue engineering, Acta Biomaterialia. 9 (2013) 7308–7319. doi:10.1016/j.actbio.2013.03.038.

[2] Y. Luo, Y. Li, X. Qin, Q. Wa, 3D printing of concentrated alginate/gelatin scaffolds with homogeneous nano apatite coating for bone tissue engineering, Materials and Design. 146 (2018) 12–19. doi:10.1016/j.matdes.2018.03.002.

[3] J. Leppiniemi, P. Lahtinen, A. Paajanen, R. Mahlberg, S. Metsä-Kortelainen, T. Pinomaa, H. Pajari, I. Vikholm-Lundin, P. Pursula, V.P. Hytönen, 3D-Printable Bioactivated Nanocellulose-Alginate Hydrogels, ACS Applied Materials and Interfaces. 9 (2017) 21959–21970. doi:10.1021/acsami.7b02756.

[4] L.S. Nair, C.T. Laurencin, Biodegradable polymers as biomaterials, Progress in Polymer Science (Oxford). 32 (2007) 762–798. doi:10.1016/j.progpolymsci.2007.05.017.

[5] C.R. Almeida, T. Serra, M.I. Oliveira, J.A. Planell, M.A. Barbosa, M. Navarro, Impact of 3-D printed PLA- and chitosan-based scaffolds on human monocyte/macrophage responses: Unraveling the effect of 3-D structures on inflammation, Acta Biomaterialia. 10 (2014) 613–622. doi:10.1016/j.actbio.2013.10.035.

[6] L.S. Nair, C.T. Laurencin, Polymers as biomaterials for tissue engineering and controlled drug delivery, Advances in Biochemical Engineering/Biotechnology. 102 (2006) 47–90. doi:10.1007/b137240.

[7] R.E. Abouzeid, R. Khiari, D. Beneventi, A. Dufresne, Biomimetic Mineralization of Three-Dimensional Printed Alginate/TEMPO-Oxidized Cellulose Nanofibril Scaffolds for Bone Tissue Engineering, Biomacromolecules. 19 (2018) 4442–4452. doi:10.1021/acs.biomac.8b01325.

[8] S.N. Pawar, K.J. Edgar, Alginate derivatization: A review of chemistry, properties and applications, Biomaterials. 33 (2012) 3279–3305. doi:10.1016/j.biomaterials.2012.01.007.

[9] J.A. Sirviö, S. Honkaniemi, M. Visanko, H. Liimatainen, Composite Films of Poly(vinyl alcohol) and Bifunctional Cross-linking Cellulose Nanocrystals, ACS Applied Materials and Interfaces. 7 (2015) 19691–19699. doi:10.1021/acsami.5b04879.

[10] R.E. Abouzeid, R. Khiari, N. El-Wakil, A. Dufresne, Current State and New Trends in the Use of Cellulose Nanomaterials for Wastewater Treatment, Biomacromolecules. 20 (2019) 573–597. doi:10.1021/acs.biomac.8b00839.

[11] N. Lin, A. Dufresne, Nanocellulose in biomedicine: Current status and future prospect, European Polymer Journal. 59 (2014) 302–325. doi:10.1016/j.eurpolymj.2014.07.025.

[12] H.P.S. Abdul Khalil, Y. Davoudpour, M.N. Islam, A. Mustapha, K. Sudesh, R. Dungani, M. Jawaid, Production and modification of nanofibrillated cellulose using various mechanical processes: A review, Carbohydrate Polymers. 99 (2014) 649–665. doi:10.1016/j.carbpol.2013.08.069.

[13] M.I. Aranguren, N.E. Marcovich, W. Salgueiro, A. Somoza, Effect of the nano-cellulose content on the properties of reinforced polyurethanes. A study using mechanical tests and positron anihilation spectroscopy, Polymer Testing. 32 (2013) 115–122. doi:10.1016/j.polymertesting.2012.08.014.

[14] J. Lu, P. Askeland, L.T. Drzal, Surface modification of microfibrillated cellulose for epoxy composite applications, Polymer. 49 (2008) 1285–1296. doi:10.1016/j.polymer.2008.01.028.

[15] J.A. Sirviö, A. Kolehmainen, H. Liimatainen, J. Niinimäki, O.E.O. Hormi, Biocomposite cellulose-alginate films: Promising packaging materials, Food Chemistry. 151 (2014) 343–351. doi:10.1016/j.foodchem.2013.11.037.

[16] Y. Shang, Y. Peng, Research of a PVA composite ultrafiltration membrane used in oil-in-water, Desalination. 204 (2007) 322–327. doi:10.1016/j.desal.2006.04.034.

[17] P. Alexy, D. Káchová, M. Kršiak, D. Bakoš, B. Šimková, Poly(vinyl alcohol) stabilisation in thermoplastic processing, Polymer Degradation and Stability. 78 (2002) 413–421. doi:10.1016/S0141-3910(02)00177-5.

[18] R.H. Schmedlen, K.S. Masters, J.L. West, Photocrosslinkable polyvinyl alcohol hydrogels that can be modified with cell adhesion peptides for use in tissue engineering, Biomaterials. 23 (2002) 4325–4332. doi:10.1016/S0142-9612(02)00177-1.

[19] T. Saito, S. Kimura, Y. Nishiyama, A. Isogai, Cellulose nanofibers prepared by TEMPO-mediated oxidation of native cellulose, Biomacromolecules. 8 (2007) 2485–2491. doi:10.1021/bm0703970.

[20] J. Sirvio, U. Hyvakko, H. Liimatainen, J. Niinimaki, O. Hormi, Periodate oxidation of cellulose at elevated temperatures using metal salts as cellulose activators, Carbohydrate Polymers. 83 (2011) 1293–1297. doi:10.1016/j.carbpol.2010.09.036.

[21] L. Rebuffi, J.R. Plaisier, M. Abdellatief, A. Lausi, A.P. Scardi, Mcx: A synchrotron radiation beamline for X-ray diffraction line profile analysis, Zeitschrift Fur Anorganische Und Allgemeine Chemie. 640 (2014) 3100–3106. doi:10.1002/zaac.201400163.

[22] J.R. Plaisier, L. Nodari, L. Gigli, E.P.R.S. Miguel, R. Bertoncello, A. Lausi, The X-ray diffraction beamline MCX at Elettra: A case study of non-destructive analysis on stained glass, Acta IMEKO. 6 (2017) 71–75. doi:10.21014/acta_imeko.v6i3.464.

[23] R.P. Chhabra, J.F. Richardson, Non-newtonian flow and applied rheology, 2008. doi:10.1016/B978-0-7506-8532-0.X0001-7.

[24] B.V.S. Jyoti, S.W. Baek, Rheological Characterization of Ethanolamine Gel Propellants, Journal of Energetic Materials. 34 (2016) 260–278. doi:10.1080/07370652.2015.1061617.

[25] K.R.N. Moelants, R. Cardinaels, R.P. Jolie, T.A.J. Verrijssen, S. Van Buggenhout, L.M. Zumalacarregui, A.M. Van Loey, P. Moldenaers, M.E. Hendrickx, Relation Between Particle Properties and Rheological Characteristics of Carrot-derived Suspensions, Food and Bioprocess Technology. 6 (2013) 1127–1143. doi:10.1007/s11947-011-0718-0.

[26] K.R.N. Moelants, R. Cardinaels, R.P. Jolie, T.A.J. Verrijssen, S. Van Buggenhout, L.M. Zumalacarregui, A.M. Van Loey, P. Moldenaers, M.E. Hendrickx, Relation Between Particle Properties and Rheological Characteristics of Carrot-derived Suspensions, Food and Bioprocess Technology. 6 (2013) 1127–1143. doi:10.1007/s11947-011-0718-0.

[27] W. Li, W.S. Chen, P.P. Zhou, L. Cao, L.J. Yu, Influence of initial pH on the precipitation and crystal morphology of calcium carbonate induced by microbial carbonic anhydrase, Colloids and Surfaces B: Biointerfaces. 102 (2013) 281–287. doi:10.1016/j.colsurfb.2012.08.042.

[28] N. Eliaz, N. Metoki, Calcium phosphate bioceramics: A review of their history, structure, properties, coating technologies and biomedical applications, Materials. 10 (2017). doi:10.3390/ma10040334.

[29] A. Salama, M. Neumann, C. Günter, A. Taubert, Ionic liquid-assisted formation of cellulose/calcium phosphate hybrid materials, Beilstein Journal of Nanotechnology. 5 (2014) 1553–1568. doi:10.3762/bjnano.5.167.